Next-generation all-solid-state battery (#ASSB)

Tuan Vo[a,b†], Claas Hüter[b], Stefanie Braun[a], Manuel Torrilhon[a]

[a]Department of Mathematics, Applied and Computational Mathematics (ACoM), RWTH Aachen University, Schinkelstraße 02, 52062 Aachen, Germany
[b]Institute of Energy and Climate Research (IEK-2), Forschungszentrum Jülich, Wilhelm-Johnen-Straße, 52428 Jülich, Germany

Mathematical modelling for the next-generation All-solid-state batteries: Nucleation (SE|SSE)$^{(*)}$-interface

Rechargeable Lithium-ion battery (LIB) is at the heart of every electric vehicle (EV), portable electronic device, and energy storage system [1]. Nowadays, LIBs enable human life more efficient and help to solve global environment issues thanks to EVs' zero emission. However, conventional LIB (c-LIB) is sensible to temperature and pressure, hence, flammable and explosive, which is undesirable. This bottleneck is mainly due to liquid-based electrolyte found in c-LIBs.

All-solid-state battery (ASSB) is one of promising candidates to overcome bottlenecks of c-LIBs. Thanks to solid-state electrolyte (SSE), ASSB is highly stable towards temperature and pressure. Nevertheless, Li-metal dendrite triggered at (SE|SSE)-interface is the main drawback of ASSB since these dendritic threads extrapolate into SSE grain boundary network, causing crevice, degradation of ionic conductivity, and the probability of short-circuit, which is unfavorable.

Next-generation All-solid-state battery (ng-ASSB) with a consideration of nucleation criterion defined by

$$a_{\text{Griffith}} := a^* = \arg\min_{a \in \mathbb{R}} \iiint_\Omega f(a, \boldsymbol{u}, \theta; \lambda, \mu, \boldsymbol{d} \otimes \boldsymbol{d})\, d\Omega - \iint_\Gamma f(a; \gamma)\, d\Gamma \Big|_{\boldsymbol{u}^{(s)}}$$

where $\boldsymbol{u}$ displacement field, θ temperature field, a crevice length, λ, μ Lame' constants, $\boldsymbol{d} \otimes \boldsymbol{d}$ embedded misorientation structural tensor, and γ cracking-surface energy density, can help to improve ASSB performance.
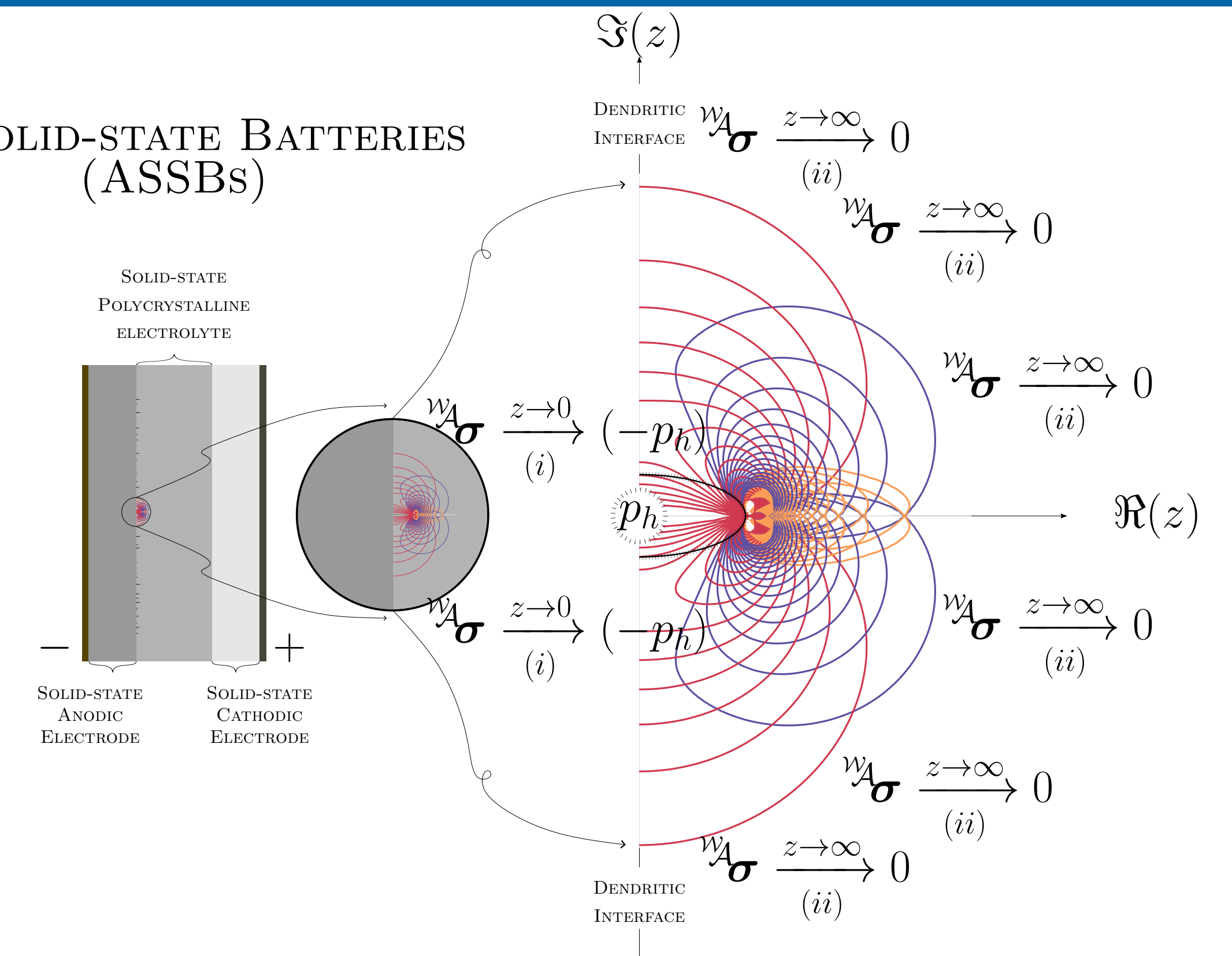
Interface Analysis

Interface between solid electrode and solid-state electrolyte (SE|SSE) taking place at space charge layer (SCL) [2] found in ASSBs critically exhibits mechanical and electrochemical instability [3]. This evidence points directly to the fact that the soft metallic li anode is erroneously prone to triggering dendrites, under cycles of electric charge & discharge [4].
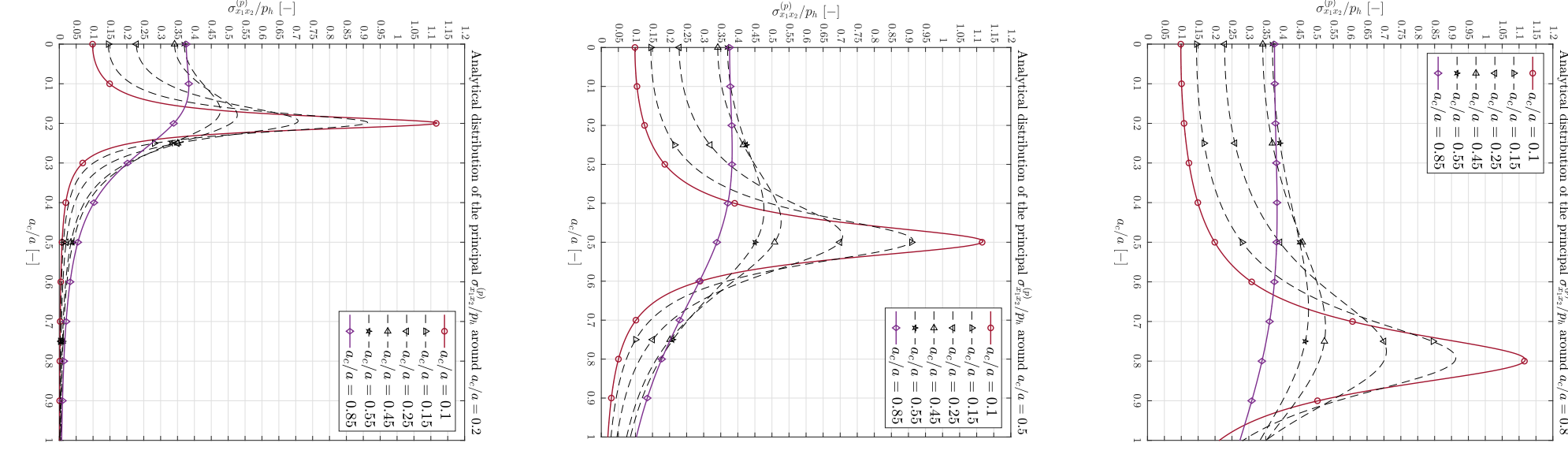
<u>Distribution</u>: ana. max. shear stress ${}^{w_A}\sigma^\Pi_{x_1 x_2}$ around crack tip a_c.

Next-generation All-solid-state battery

Nucleation taking place at critical dendritic (SE|SSE)-interface
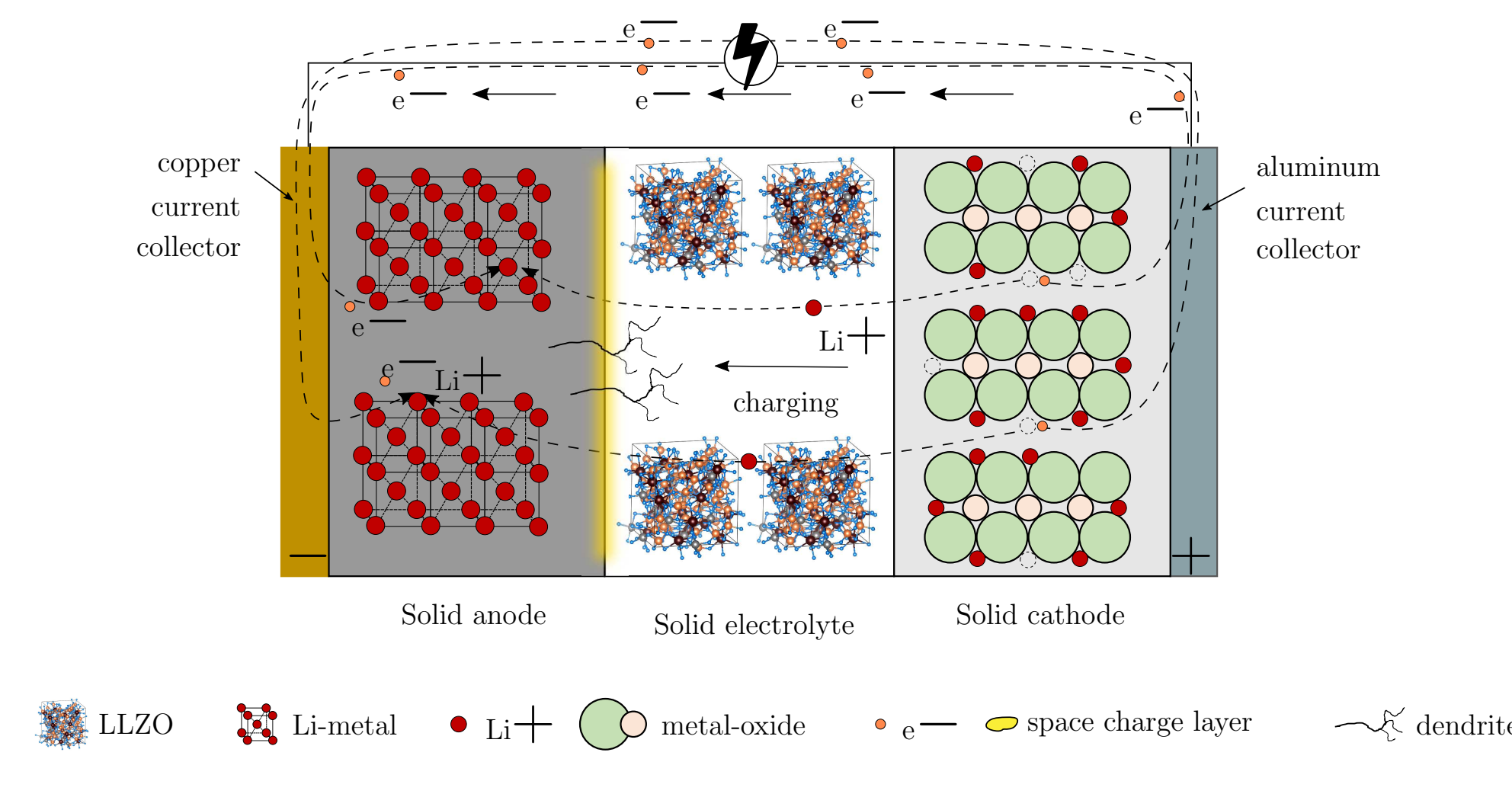
Thermodynamic consistency: satisfied.
Closure problem: fulfille by 15 moments.

Embedded structural-tensor SSE

Polycrystalline garnet-typed SSE such as LLZO exhibit a network of grain boundaries, and grains with various sizes and shapes under microscopic observation. Therefore, this type of microstructure is potentially prone to nuance destruction of ceramic-like materials.
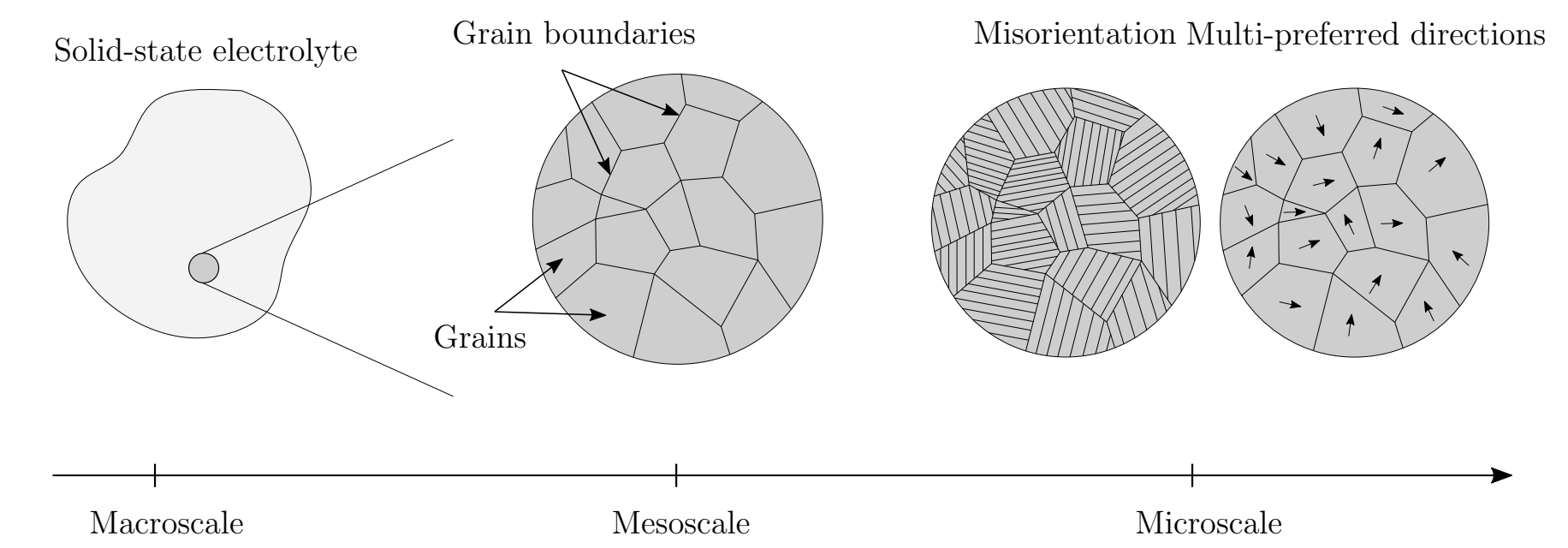
Consequentially, dendrites contribute to degradation of ionic conductivity and cracks via tracing along grain boundaries.

Nucleation interface: Taking place at the critical dendritic interface

Coupled fields: Displacement vector field and temperature scalar field

$$\boldsymbol{u} : \begin{cases} \Omega \times \mathbb{R}_+ \to \mathbb{R}^3, \\ (\boldsymbol{x}, t) \mapsto \boldsymbol{u}(\boldsymbol{x}, t), \end{cases} \quad \theta : \begin{cases} \Omega \times \mathbb{R}_+ \to \mathbb{R}, \\ (\boldsymbol{x}, t) \mapsto \theta(\boldsymbol{x}, t), \end{cases} \quad \theta : \begin{cases} \Omega \times \mathbb{R}_+ \to \mathbb{R}, \\ (\boldsymbol{x}, t) \mapsto \theta(\boldsymbol{x}, t), \end{cases}$$

Governing conservation equations

$$\frac{d}{dt} \int_\Omega (\cdot)\, d\Omega = \int_\Omega (\cdot)^{\text{action}}\, d\Omega + \int_{\partial\Omega} (\cdot)^{\text{action}}\, d\partial\Omega + \int_\Omega (\cdot)^{\text{production/source/sink}}\, d\Omega$$

$\rho(\boldsymbol{x}, t)$ is mass density per unit volume (puv); $\boldsymbol{b}(\boldsymbol{x}, t)$ body force puv; $\boldsymbol{v}(\boldsymbol{x}, t)$ velocity; $e(\boldsymbol{x}, t)$ internal energy puv; $\boldsymbol{q}(\boldsymbol{x}, t)$ heat flux; $r(\boldsymbol{x}, t)$ heat source puv; $\boldsymbol{\sigma}$ Cauchy stress and $\boldsymbol{\varepsilon}$ infinitesimal strain. Helmholtz energy functional

$$a_{\text{Griffith}} := a^* = \arg\min_{a \in \mathbb{R}} \iiint_\Omega f(a, \boldsymbol{u}; \lambda, \mu, \boldsymbol{d} \otimes \boldsymbol{d})\, d\Omega - \iint_\Gamma f(a; \gamma)\, d\Gamma \Big|_{\boldsymbol{u}^{(s)}}$$

Governing PDE

$$a_{\text{Griffith}} := a^* = \arg\min_{a \in \mathbb{R}} \iiint_\Omega f(a, \boldsymbol{u}; \lambda, \mu, \boldsymbol{d} \otimes \boldsymbol{d})\, d\Omega - \iint_\Gamma f(a; \gamma)\, d\Gamma \Big|_{\boldsymbol{u}^{(s)}}$$

abc

Strain energy: Interface between solid electrode and solid-state electrolyte (SE|SSE) taking place at space charge

$$\iiint_\Omega f(a, \boldsymbol{u}; \lambda, \mu, \boldsymbol{d} \otimes \boldsymbol{d})\, d\Omega$$

Surface energy: Interface between solid electrode and solid-state electrolyte (SE|SSE) taking place
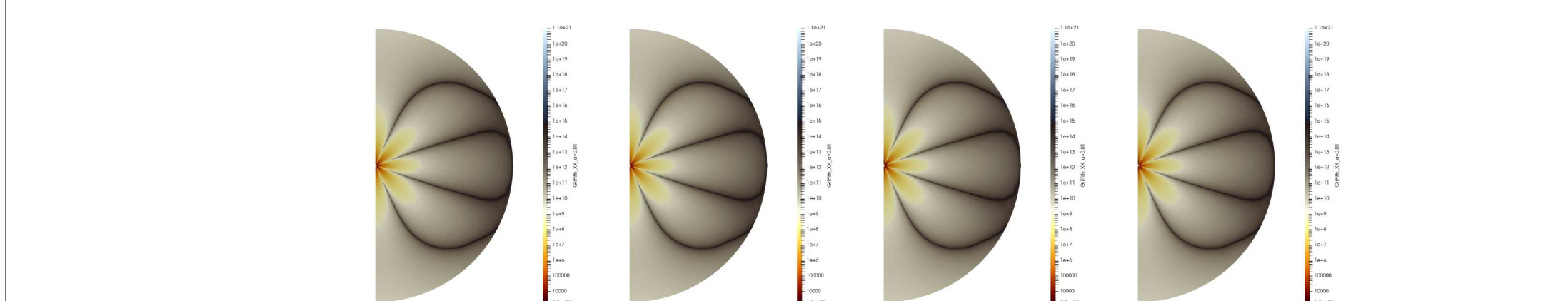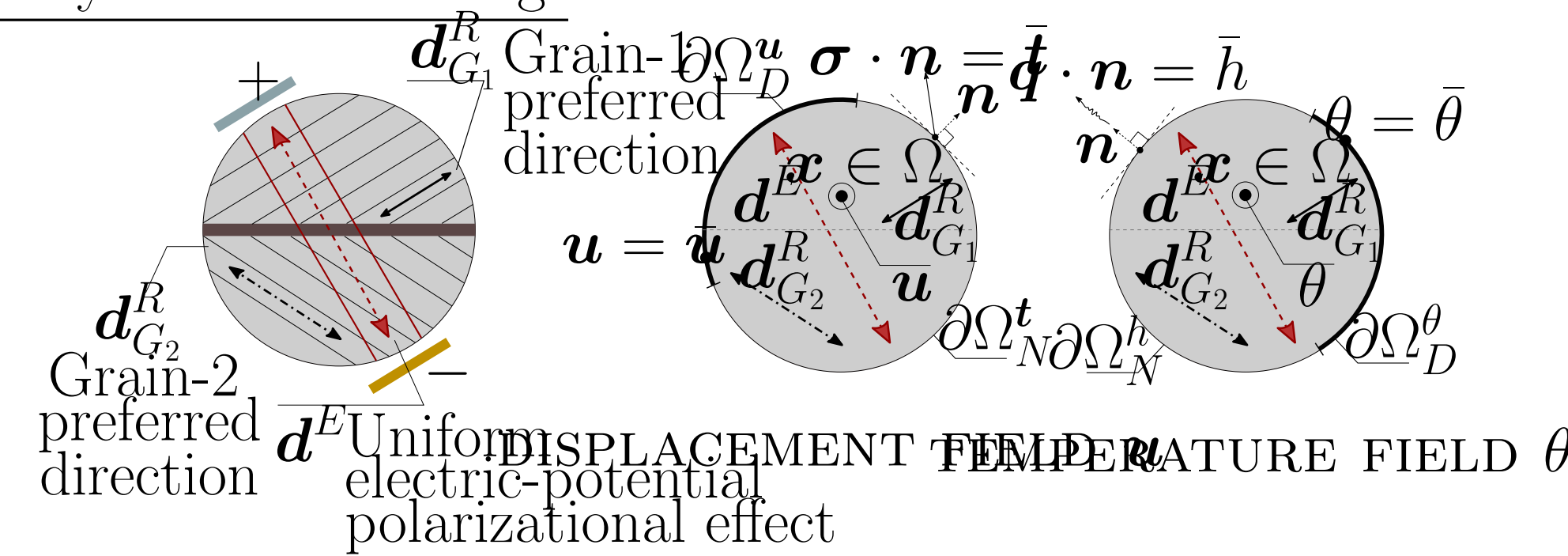
$$\iint_\Gamma f(a; \gamma)\, d\Gamma$$

Therefore

$$\rho\, \partial_{t^2}^2 \boldsymbol{u}^{(s)} + \nabla \cdot \left(\overset{4}{\mathbb{C}} {}^{\mathrm{D}(\Omega)}_{J(\lambda,\mu)} : \nabla \boldsymbol{u}^{(s)} \right) + \rho \nabla V_e = \boldsymbol{0},$$

s.t. $\quad a_{\text{Griffith}} := a^* = \arg\min_{a \in \mathbb{R}} \iiint_\Omega f(a, \boldsymbol{u}; \lambda, \mu, \boldsymbol{d} \otimes \boldsymbol{d})\, d\Omega - \iint_\Gamma f(a; \gamma)\, d\Gamma \Big|_{\boldsymbol{u}^{(s)}}$

abc

Boundary condition settings

$\boldsymbol{d}^R_{G_1}$ Grain-1 preferred direction
$\partial\Omega^{\boldsymbol{u}}_D$ $\boldsymbol{\sigma} \cdot \boldsymbol{n} = \bar{\boldsymbol{t}}$ $\bar{\boldsymbol{q}} \cdot \boldsymbol{n} = \bar{h}$ $\theta = \bar{\theta}$
$\boldsymbol{d}^R_{G_2}$ Grain-2 preferred direction
$\boldsymbol{d}^E$ Uniform electric-potential polarizational effect

DISPLACEMENT FIELD $\boldsymbol{u}$ TEMPERATURE FIELD θ

Comparison: Analytical vs. Numerical solutions
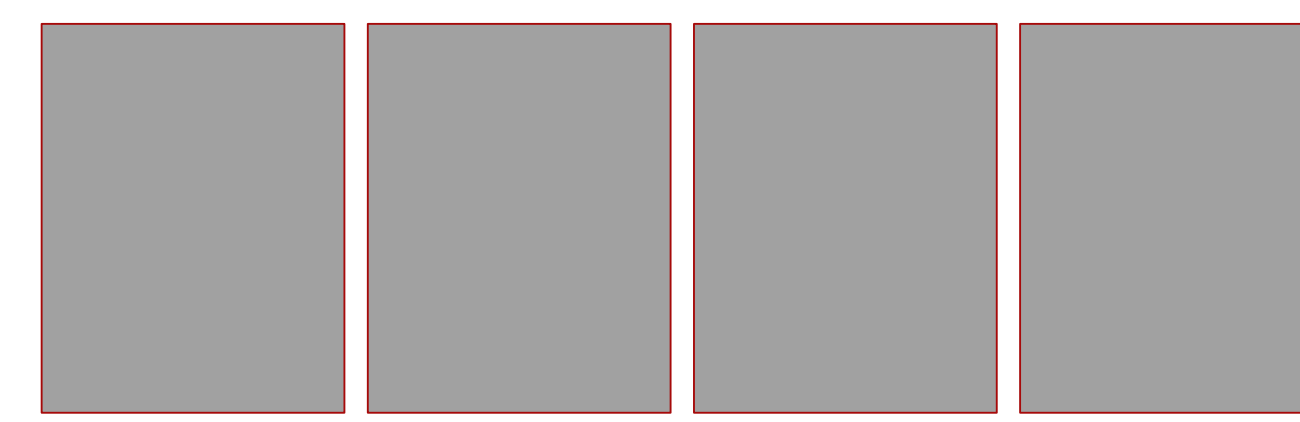
Airy-Westergaard function used for max. shear stress analysis

$${}^{w}\!\mathcal{A} : \mathbb{C} \to \mathbb{C}, z \mapsto {}^{w}\!\mathcal{A}(z) := \Re\left(\oiint_\Gamma \mathcal{K}^{(\star)}\, dz \right) + x_2 \Im\left(\oint_\Gamma \mathcal{K}^{(\star)}\, dz \right), \mathcal{K}^c(z) := -p_h + p_h/\sqrt{1 - a^2/z^2},$$

where $\{p_h, a\} \in \mathbb{R}_+$ is the.

FEM implementation: element matrix $\boldsymbol{K}^e$ approx. by *Gauss quadrature*; indices imply $4+2=6$ *for-loop*:

$$K^{\alpha\beta}_{ik} = \int_{\Omega^\xi} \left(\mathcal{L}^\alpha_1\, \mathbb{C}^{fGL}_{i1k1}(y)\, \mathcal{R}^\beta_1 + \mathcal{L}^\alpha_1\, \mathbb{C}^{fGL}_{i1k2}(y)\, \mathcal{R}^\beta_2 + \mathcal{L}^\alpha_2\, \mathbb{C}^{fGL}_{i2k1}(y)\, \mathcal{R}^\beta_1 + \mathcal{L}^\alpha_2\, \mathbb{C}^{fGL}_{i2k2}(y)\, \mathcal{R}^\beta_2 \right) \det(\boldsymbol{J})\, d\Omega^\xi$$

where $\mathcal{L}^\alpha_j$ and $\mathcal{R}^\beta_l$ are gradients of basis functions at node α^{th} and β^{th}, respectively.

FEM: Strain energy density

Partial differential equation
$$\nabla \cdot \left(\mathbb{C}^{fGL}(y) \nabla_s \boldsymbol{u} \right) + \rho \boldsymbol{b} = 0$$

Displacement solution
$$u_i$$

Strain
$$\varepsilon_{ij} = \frac{1}{2}\left(u_{i,j} + u_{j,i} \right)$$

Stress
$$\sigma_{ij} = \mathbb{C}^{fGL}_{ijkl}(y)\, \varepsilon_{kl}$$

Strain energy density
$$\mathcal{E}_{\text{strain}} := \frac{1}{2}\sigma_{ij}\varepsilon_{ij}$$

abc
abc

Contact

Tuan Vo
vo@acom.rwth-aachen.de

Scan me

References

[1] **T.Vo**, *Modeling the swelling phenomena of li-ion batt. cells based on a numerical chemo-mech. coupled approach*. MA, Robert Bosch Battery Systems GmbH, 2018.

[2] **S.Braun**, C.Yada and A.Latz, *Thermodynamically consistent model for Space-Charge-Layer formation in a solid electrolyte*. Jr. Phys. Chem., 119, 22281-22288, 2015.

[3] **C.Hüter**, S.Fu, M.Finsterbusch, E.Figgemeier, L.Wells, and R.Spatschek, *Electrode-electrolyte interface stability in solid state electrolyte system: influence of coating thickness under varying residual stresses*. AIMS Materials Science, 4(4):867-877, 2017.

[4] **S.Kim**, J.S.Kim, L.Miara, Y.Wang, S.K.Jung, S.Y.Park, Z.Song, H.King, M.Badding, J.M.Chang, V.Roev, G.Yoon, R.Kim, J.H.Kim, K.Yoon, D.Im, and K.Kang, *High-energy and durable li metal batt. using garnet-type solid electrolytes with tailored li-metal compatibility*. Nature Communications, 13(1):1883, 2022.